DAC-Less PAM-4 Slow-Light Silicon Photonic Modulator Assisted by Coupled Bragg Grating Resonators

Omid Jafari[1,*], Sasan Zhalehpour[2], Wei Shi[1], and Sophie LaRochelle[1]
[1]*Centre d'optique, photonique et laser (COPL), Université Laval, Québec City, QC, Canada*
[2]*Canada research center, Huawei Technologies Canada, Ottawa, ON, Canada*
Omid.jafari.1@ulaval.ca

Abstract: We report a slow-light all-silicon modulator with two segmented electrodes that enables high-speed-PAM operations and simultaneously meets all requirements of high bandwidth (>40GHz), power-efficient operation (73fJ/bit), compact footprint ($L_{SL\text{-}MZM}$=570µm), and wide operating wavelength range ($\Delta\lambda$=2nm).

1. Introduction

Silicon photonic (SiP) platform has emerged as an enabling technology to realize high-performance transceivers with a cost-effective implementation [1]. The key driving force behind SiP technology lies in the compatibility with mature complementary metal-oxide-semiconductor (CMOS) manufacturing processes. Rapidly growing demands in data centers necessitate optical transceivers composed of SiP modulators that can simultaneously achieve high bandwidth, high power efficiency, compact footprint, and stability. Providing a compromise between data rate and complexity, pulse amplitude modulation (PAM) has been used to increase transmission speed in short-reach links. Compared to the quadrature amplitude modulation (QAM), PAM exploits direct detection to offer less complex receiver (less cost) and keep the required power budget low [1]. To achieve PAM operations, SiP modulators with multiple electrodes, acting as an optical DAC, have been reported in Mach-Zehnder modulators (MZMs) [2] and micro-ring modulators (MRMs) [3]. However, MZMs are energy hungry and have a large footprint, whereas MRMs suffer from their narrow operating bandwidth and output chirp.

In this paper, we demonstrate a SiP modulator that offers a high modulation efficiency and stable operation. We report on an MZM assisted by integrated Bragg grating resonators (IBGRs) [4]. IBGRs enhance optical phase modulation in each arm of the MZM by slowing down optical waves over a nm-scale wavelength range, which allows for a more compact footprint and higher modulation efficiency than conventional MZMs, while offering a more robust operation compared to MRM in presence of temperature fluctuation [4]. PAM-4 signals are generated employing segmented electrodes driven with two binary signals, eliminating the need for a high-speed electrical DAC (DAC-less operation). The modulator combines the advantages of low energy consumption (E_b = 73 fJ/bit), large electro-optic bandwidth (> 40 GHz), and high-speed operation (up to 90 Gb/s with a bit error rate (BER) below 20 % FEC threshold) over a spectral bandwidth ($\Delta\lambda$ = 2 nm) much larger than usual resonator-based modulators.

2. Modulator design

Figures 1 (a) and (b) display the schematic of the segmented MZM assisted by IBGRs and its cross-section. Bragg gratings are designed by sidewall corrugations with a duty cycle of 50%, a uniform period of Λ = 300 nm, a maximum/minimum width of 1000 nm/250 nm in a partial etch waveguide (slab height of 90 nm and ridge of 220 nm). Each resonator, engineered with a low Q-factor, is composed of a phase-shifted section (shown in figure

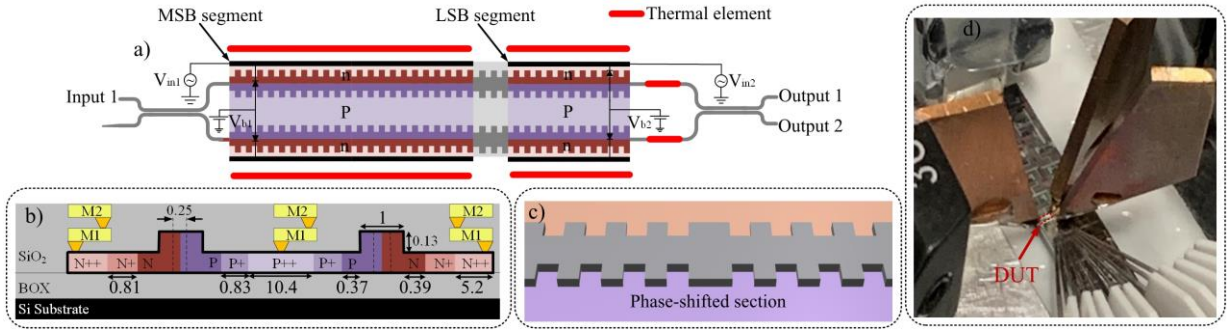

Fig. 1. (a) Schematic of the DAC-less PAM-4 SL-MZM, (b) cross-section of the modulator (the labeled parameters are in µm), (c) schematic of a phase-shifted Bragg grating resonator, and (d) modulator under the test.

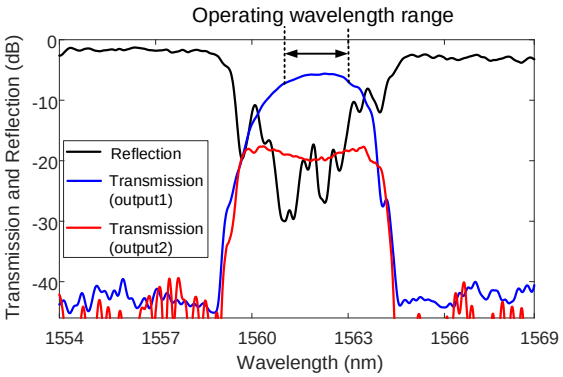

Fig. 2. Transmission and reflection spectra of the IBGRs-assisted MZM zoomed on the resonance wavelength

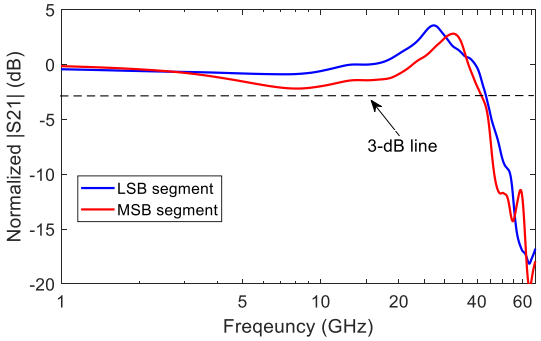

Fig. 3. Electro-optic response of the LSB segment and MSB segment at the bias voltage of zero.

1 (c)) and 38 periods on each side. Then, multiple of these resonators are cascaded in each arm to form IBGRs. We introduced 26 phase-shifted sections along the Bragg grating waveguide, *i.e.*, an IBGR design with 26 coupled resonators. The two segments, called "most significant bit (MSB) segment" and "least significant bit (LSB) segment", are respectively formed by 15 and 10 of these resonators loaded with p-n junctions. Therefore, one resonator is unloaded in order to eliminate the RF leakage power between the MSB and LSB segments.

Since the coupled cavities resonate at almost the same wavelength, it is not necessary to tune them independently. Therefore, we only placed four thermal elements (see figure 1 (a)), on top of each segment, to fine-tune response if necessary. This is an advantage of this design compared to the slow-light design based on cascaded micro-ring resonators which are inherently uncoupled resonators and require an independent tuning mechanism [5]. Also, compared to the slow-light photonic crystal waveguides (PCWs) [6], Bragg grating designs ease the requirement on minimum feature sizes of fabrication processes and therefore, they are routinely fabricated with standard manufacturing processes.

3. Measurement results

The modulator was fabricated in a multi-project wafer run using a standard 193-nm lithography process at the IME (AMF) A*STAR with a silicon layer thickness of 220 nm and a 2 µm buried oxide. Figure 1 (d) shows the modulator under test. It has a compact footprint (a phase shifter length of $L_{SL\text{-}MZM}$ = 570 µm). Figure 2 presents the modulator transmission and reflection spectra near the resonance wavelength. The transmission bandwidth at the IBGR stopband is 3.2 nm. The resonance bandwidth is much larger than that of single-resonance-based modulators, *e.g.*, MRMs (~ 0.1 nm). This is a result of employing a number of coupled low-Q-factor resonators. Figure 2 also indicates that the insertion loss is 5.5 dB. The two slow-light phase shifters record a $V_\pi \times L$ of 0.51 Vcm. Compared with conventional phase shifters that are fabricated with the same process, the slow-light phase shifters provide an enhancement factor of 6 in phase modulation.

We measured the electro-optic response of the modulator using a PNA Microwave Network Analyzer (Agilent N5227A 10 MHz - 67 GHz) and 50-Ω terminated RF probes. Figure 3 shows the EO response of modulator at a zero-voltage bias. Both MSB segment (red line) and LSB segment (blue line) obtain a 3-dB electro-optic bandwidth of > 40 GHz. The electro-optic response is limited by the RC time constant as well as the slow-light effect, despite the small the low photon life time introduced by low-Q-factors resonators [7].

Figure 4 shows the schematic of the measurement setup to evaluate the BER. We first generated a PRBS with a length of 2^{15}-1, amplified the RF signal applied to the MSB (LSB) segment using RF amplifier with a bandwidth of 30 GHz (40 GHz) and a peak-to-peak voltage of 7 V_{pp} (6 V_{pp}). The laser power was 15 dBm and polarization was adjusted with a polarization controller (PC) before coupling into the chip. After modulation, the signal was amplified by a two-stage EDFA (each stage followed by a tunable optical bandpass filter), detected using a 32 GHz photodetector, and captured by a 63 GHz real-time oscilloscope (RTO) with a sampling rate of 80GSa/s. At the receiver side, we performed offline digital signal processing (DSP) as shown in the table in figure 4. The signal is filtered by a 10^{th} order super Gaussian low pass filter (LPF), resampled, and down-sampled. BER is calculated using a decision-directed minimum mean square error (DD-MMSE) equalizer with a tap number of 2^4. The signal also is de-mapped and time synchronized for BER calculation.

Figure 5 reports the BER performance when generating PAM-4 signals by applying electrical signals to both MSB and LSB segments at λ_0 = 1561 nm, λ_0 = 1562 nm, and λ_0 = 1563 nm. Over the 2-nm operating wavelength range, the BER is less than the 20 % FEC threshold up to 90 Gb/s (reverse bias of 1.5 V). Therefore, the modulator

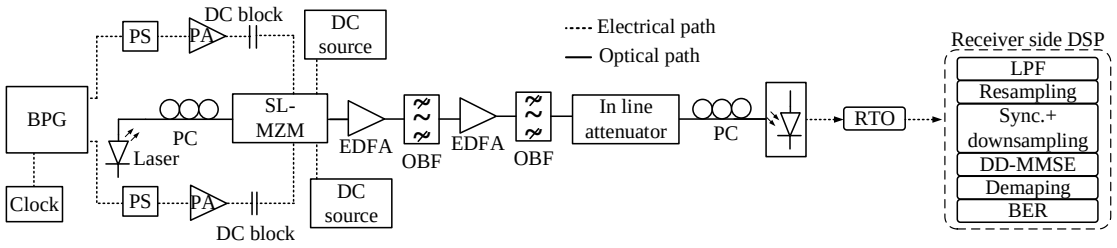

Fig. 4. The measurement setup demonstrating the optical and electrical components along with the off-line DSP block diagram at the reception.

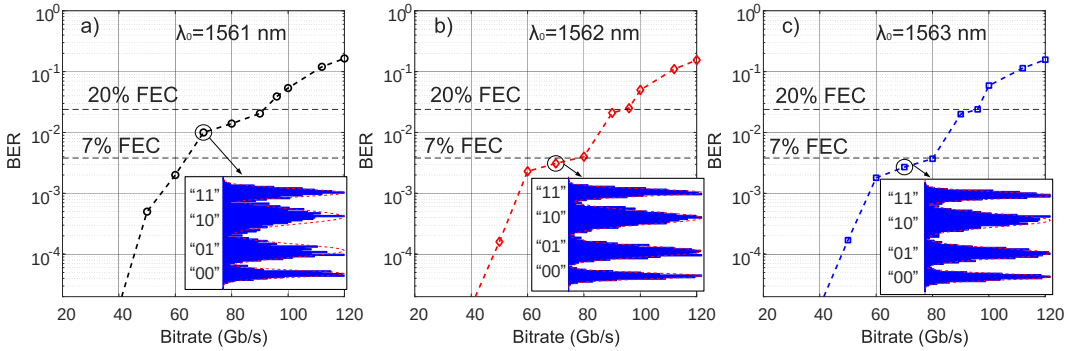

Fig. 5. BER measurement of the DAC-less IBGRs-assisted MZM for PAM-4 format for an operating wavelength of a) 1561 nm, b) 1562 nm, and c) 1563 nm at a reverse bias voltage of 1.5 V. The insets show the histograms of detected bits (one sample per symbol) used for BER calculation at a bitrates of 70 Gb/s. The dashed red lines in the insets show the Gaussian distributions.

offers one order of magnitude larger operating wavelength range compared to MRMs. This avoids the strong dependence of the frequency response on frequency detuning, which results in a dynamic nonlinear response observed in MRMs. Also, the 2-nm operating range guaranties stability in the presence of temperature fluctuations within ΔT = 50 °C (considering a heterogeneously integrated laser with 40 pm/°C wavelength drift between laser and SiP modulators [3]). The insets in figure 5 show the histograms of detected bits (one sample per symbol) used for BER calculation at 70 Gb/s. Driven by single-derive push-pull configuration with lumped electrodes, the modulator consumes an estimated total energy of 73 fJ/bit for PAM-4 format [1].

4. Conclusion

We demonstrated a slow-light SiP modulators for generating PAM-4 signals without the need for electrical DACs. IBGRs are loaded into each arm of the MZM to enhance the phase modulation over a relatively large optical bandwidth. The modulator is charactized by $V_\pi \times L$ of 0.51 Vcm, an energy consumpton of 73 fJ/bit, and an electro-optic bandwidth of > 40 GHz. The modulator demonstrates operations up to 90 Gb/s over a 2-nm operating wavelength range, corresponding to ΔT = 50 ^{0}C.

5. Acknowledgements

This project was supported by The NSERC of Canada and Huawei Canada through a partnership grant (CRDPJ 538381-18). The authors also thank CMC Microsystems for the fabrication subsidy and MPW service.

6. References

1. W. Shi, Y. Xu, H. Sepehrian, S. Larochelle, and L. A. Rusch, "Silicon photonic modulators for PAM transmissions," J. Opt. (United Kingdom) **20**, 083002 (2018).
2. A. Samani, D. Patel, M. Chagnon, E. El-Fiky, R. Li, M. Jacques, N. Abadía, V. Veerasubramanian, and D. V. Plant, "Experimental parametric study of 128 Gb/s PAM-4 transmission system using a multi-electrode silicon photonic Mach Zehnder modulator," Opt. Express **25**, 13252 (2017).
3. J. Sun, R. Kumar, M. Sakib, J. B. Driscoll, H. Jayatilleka, and H. Rong, "A 128 Gb/s PAM4 Silicon Microring Modulator With Integrated Thermo-Optic Resonance Tuning," J. Light. Technol. **37**, 110–115 (2019).
4. O. Jafari, W. Shi, and S. Larochelle, "Mach-Zehnder Silicon Photonic Modulator Assisted by Phase-Shifted Bragg Gratings," IEEE Photonics Technol. Lett. **32**, 445–448 (2020).
5. S. Romero-García, A. Moscoso-Mártir, S. S. Azadeh, J. Müller, B. Shen, F. Merget, and J. Witzens, "High-speed resonantly enhanced silicon photonics modulator with a large operating temperature range," Opt. Lett. **42**, 81–84 (2017).
6. Y. Terada, K. Kondo, R. Abe, and T. Baba, "Full C-band Si photonic crystal waveguide modulator," Opt. Lett. **42**, 5110–5112 (2017).
7. O. Jafari, W. Shi, and S. Larochelle, "Efficiency-speed tradeoff in slow-light silicon photonic modulators," IEEE J. Sel. Top. Quantum Electron. 1–1 (2020).